

Quadriexciton binding energy in electron-hole bilayers

Cesare Malosso ¹  Gaetano Senatore ²  and Stefania De Palo ^{2,3} *

¹ SISSA – Scuola Internazionale Superiore di Studi Avanzati, 34136 Trieste, Italy; cmalosso@sissa.it

² Dipartimento di Fisica, Università di Trieste, strada Costiera 11, 34151 Trieste, Italy; senatore@units.it

³ CNR-IOM-DEMOCRITOS, Trieste, Italy; depalo@iom.cnr.it

* Correspondence: senatore@units.it, (S.D.P)

Abstract: Excitonic condensation and superfluidity have recently received a renewed attention, due to the fabrication of bilayer systems in which electrons and hole are spatially separated and form stable pairs known as indirect excitons. Dichalcogenides- and graphene- based bilayers are nowadays built and investigated, giving access to systems with (i) only spin degeneracy, (ii) spin and valley degeneracy. Simulation studies performed in the last decade at $T = 0$ for simple, model electron-hole bilayers, as function of inter-layer distance and in-layer carrier density, have revealed in case (i) the formation of biexcitons in a tiny region of parameter space and in case (ii) the formation of stable compounds made of 4 electrons and 4 holes (quadriexcitons) in a sizable region of parameter space. Of some interest is the relation of the properties of isolated biexcitons (quadriexcitons) and those of their finite density counterpart. In fact, the isolated biexciton has been repeatedly studied in the last years with simulations and other techniques. No simulations, instead, are available to our knowledge for the isolated quadriexciton, for which we present here results of the first quantum Monte Carlo (QMC) study. Stability with respect to the dissociation into biexcitons, and the pair correlations with varying the inter-layer distance d are discussed.

Keywords: Exciton; , Quadriexciton; Binding energy , Quantum Monte Carlo

1. Introduction

An exciton [1,2], a bound electron-hole pair in a semiconductor, is an elementary optical excitation or quasiparticle in solid state physics, reminiscent of positronium or hydrogen in atomic physics. Interactions between two excitons can result in the formation of an excitonic molecule [3,4], a new quasi-particle known as biexciton [4]. The study of excitons and biexcitons is most naturally performed within the envelope function and effective mass approximations [5], which provide an effective hamiltonian for interacting electron and hole quasiparticles, near energy band extrema. Whenever a band has multiple equivalent minima (maxima) the description of electrons (holes) implies a new discrete quantum number, the valley index v , which identifies a minimum (maximum). The valley index can be formally treated as a pseudospin; the number g_v of equivalent valleys fixes the length τ of the pseudospin, $2\tau + 1 = g_v \rightarrow \tau = (g_v - 1)/2$. We can introduce a flavor (or valley-spin) index $\sigma = (\tau_z, s_z)$ to fix the spin and pseudospin states. As electrons and holes have spin $1/2$, the total number of flavors is $N_c = 2g_v$ for each particle type, electron or hole. We shall assume that the Hamiltonian does not contain spin or pseudospin operators. It is evident that if one considers a finite electron-hole system with $N_e \leq N_c$, $N_h \leq N_c$, with N_e (N_h) the number of electrons (holes), the ground state wavefunction Φ can be exactly factorized in $\Phi = \Psi\zeta$, with Ψ a nodeless wavefunction of the particles cartesian coordinates and ζ a wavefunction of pseudospin and spin coordinates; Ψ will be symmetric for any pair exchange of electrons (holes) coordinates and ζ will be antisymmetric for any pair exchange of electrons (holes) coordinates. One can of course choose Ψ to have also other symmetries possessed by the hamiltonian, provided that this does not spoil the exchange symmetry and Ψ remains nodeless.



Citation: . Preprints 2022, 1, 0.
<https://doi.org/>



Copyright: © 2022 by the authors. Licensee MDPI, Basel, Switzerland. This article is an open access article distributed under the terms and conditions of the Creative Commons Attribution (CC BY) license (<https://creativecommons.org/licenses/by/4.0/>).

Long ago it was observed [6] that, when there are g_v equivalent minima in the electron conduction band, up to $N_c = 2g_v$ electrons can occupy the same molecular orbital and therefore electron-hole complexes with up to N_c excitons are possible; the same being true [6] when N_c equivalent maxima are present in the valence band. Clearly, in a system with $g_v = 2$, such as coupled graphene bilayers [7–12], $N_c = 4$ and quadriexcitons should be possible. We recall that the problem of an isolated biexciton has been already studied [13–15] with DMC and other techniques.

Before tackling below the treatment of an isolated quadriexciton (or biexciton) at $T = 0$, in the simplest, model electron-hole bilayer (the paramagnetic, symmetric bilayer: $m_e^* = m_h^* = m_b$), we briefly summarize here the results of available QMC simulations of systems with finite in-layer carrier density n [16–18], which we specify via the dimensionless r_s parameter, defined by $\pi^2 r_s^2 a_B^2 = 1/n$ where $a_B^* = 4\pi\epsilon_0\epsilon\hbar^2/(m_b e^2)$.

The first simulations [16] were performed in the region of parameter space $0 < d/(r_s a_B^*) \leq 3$, $0 \leq r_s \leq 30$ with $g_v = 1$. It was found that at large density $r_s \lesssim 1$ the plasma phase is stable at all distances d , due to the screening of the Coulomb attraction by carriers. Increasing r_s an excitonic condensate appear for $d < d_X(r_s)$ with $d_X(r_s)$ an increasing function of r_s . For $d > d_X(r_s)$ the plasma phase is stable up to intermediate density, $r_s \lesssim 20$, while turning into a Wigner crystal for $20 \lesssim r_s \lesssim 30$. More recent simulations [17], performed in a much smaller region of parameter space ($0 < d/a_B^* \leq 4$, $0 \leq r_s \leq 8$) with $g_v = 1$, using a much more flexible wavefunction and up to date computer resources, confirm semiquantitatively the phase boundary between the excitonic and plasma phases as well as the condensate fractions found in [16], while finding for $4 \lesssim r_s \lesssim 8$ a new, stable biexcitonic phase for $d \lesssim d_{2X}(r_s) = 0.05a_B^*$. Finally, the results of QMC simulations for an electron-hole bilayer with $g_v = 2$ and $0 < d/a_B^* \leq 3.5$, $0 \leq r_s \leq 8$ have just been published. [18]. As predicted by [6] a quadriexcitonic phase is found and in a sizeable region of parameter space, compared with the region of stability of the biexcitonic phase found for $g_v = 1$. The new phase appears for $r_s \gtrsim 1$ and $0 \lesssim d/ \lesssim d_{4X}(r_s)$, with $d_{4X}(r_s)$ an increasing function of r_s . At given $r_s \gtrsim 1$ and for $d_{4X}(r_s) \lesssim d \lesssim d_X(r_s)$ there is the excitonic phase, followed by the plasma phase for $d \gtrsim d_X(r_s)$. No trace is found of the biexcitonic phase.

2. Hamiltonians and wave functions

Within the envelope function-effective mass approximation [5] the Hamiltonian of a 2-dimensional bilayer reads

$$\begin{aligned}
 H = & - \frac{\hbar^2}{2m_e^*} \sum_{v,i} \nabla_{e,v,i}^2 + \frac{1}{2} \sum'_{v,v',i,i'} \frac{1}{|\mathbf{r}_{e,v,i} - \mathbf{r}_{e,v',i'}|} - \frac{\hbar^2}{2m_h^*} \sum_{v,i} \nabla_{h,v,i}^2 + \frac{1}{2} \sum'_{v,v',i,i'} \frac{1}{|\mathbf{r}_{h,v,i} - \mathbf{r}_{h,v',i'}|} \\
 & - \sum_{v,v',i,i'} \frac{1}{\sqrt{|\mathbf{r}_{e,v,i} - \mathbf{r}_{h,v',i'}|^2 + d^2}}.
 \end{aligned} \tag{1}$$

This Hamiltonian, apart from the assumption of isotropic masses is quite general: v and v' run over the valleys and i and i' run over the number of electrons or hole in a given valley. A prime in the sum excludes terms with both $v = v'$ and $i = i'$. The paramagnetic, symmetric bilayer is the one in which $m_h^* = m_e^* = m_b$, all valleys present have the same electron (hole) population and in each valley there is the same number of spin up and spin down electrons (holes). In the rest of this paper we measure distances using the effective Bohr radius $a_B^* = 4\pi\epsilon_0\epsilon\hbar^2/(m_b e^2)$ and energies in effective Rydbergs $Ry^* = \hbar^2/(2m_b a_B^{*2})$, so that the Hamiltonian becomes

$$\begin{aligned} \mathcal{H} = & - \sum_{v,i} \nabla_{e,v,i}^2 + \sum'_{v,v',i,i'} \frac{1}{|\mathbf{r}_{e,v,i} - \mathbf{r}_{e,v',i'}|} - \sum_{v,i} \nabla_{h,v,i}^2 + \sum'_{v,v',i,i'} \frac{1}{|\mathbf{r}_{h,v,i} - \mathbf{r}_{h,v',i'}|} \\ & - \sum_{v,v',i,i'} \frac{2}{\sqrt{|\mathbf{r}_{e,v,i} - \mathbf{r}_{h,v',i'}|^2 + d^2}}. \end{aligned} \quad (2)$$

As we have argued above for $N_e = N_h = N_c \equiv N$ the ground-state wave function $\Psi_{NX}^0(\mathbf{R}_e, \mathbf{R}_h)$, with \mathbf{R}_e (\mathbf{R}_h) the electrons (holes) coordinates, (i) must be solution of

$$\mathcal{H}\Psi_{NX}^0(\mathbf{R}_e, \mathbf{R}_h) = E_{NX}^0\Psi_{NX}^0(\mathbf{R}_e, \mathbf{R}_h); \quad (3)$$

(ii) must be symmetric for any pair exchange of electron (holes) coordinates; (iii) in the symmetric bilayer must be symmetric for electron-hole exchange, i.e., $\Psi_{NX}^0(\mathbf{R}_e, \mathbf{R}_h) = \Psi_{NX}^0(\mathbf{R}_h, \mathbf{R}_e)$ [13].

For the biexciton and the quadriexciton we have tackled the problem in eq. (3) resorting to variational and diffusion Monte Carlo [19–21] (VMC and DMC) as implemented in our own code. For given N , at each d an optimal trial function $\Psi_{NX}^T(\mathbf{R}_e, \mathbf{R}_h; \mathbf{c})$ is determined by minimizing the variational energy with respect to a number of optimizable parameters \mathbf{c} [22]. We then compute VMC estimates of the properties of interest using Monte Carlo integration with $|\Psi_{NX}^T|^2$ as the importance function; DMC estimates are obtained employing the optimised Ψ_{NX}^T as the guiding function. We now turn to the explicit form of Ψ_{NX}^T .

2.1. Polyexciton wave function Ψ_{NX}^T

Here we restrict to polyexcitons made by N_e electrons and N_e holes. Given the symmetry requests on the wave function it is natural to write $\Psi_{NX}^T(\mathbf{R}_e, \mathbf{R}_h)$ as a symmetrized Jastrow factor. We start from the unsymmetrized form

$$J(\mathbf{R}_e, \mathbf{R}_e) = \exp \left[-(1/2) \sum_{\mu, \mu'} \sum'_{i_\mu, j_{\mu'}} u_{\mu, \mu'} (|\mathbf{r}_{i_\mu} - \mathbf{r}_{j_{\mu'}}|) \right], \quad (4)$$

embodying two-body pseudo potentials among all particles. Above the *species* index $\mu = (t, \sigma)$ combines the particle type ($t = e, h$) and the flavor $\sigma = (\tau_z, s_z)$; moreover, the primed sum for $\mu' = \mu$ contains only the terms with $i_\mu \neq j_\mu$. Evidently

$$J(\mathbf{R}_e, \mathbf{R}_e) = J_{ee}(\mathbf{R}_e) J_{hh}(\mathbf{R}_h) J_{eh}(\mathbf{R}_e, \mathbf{R}_h). \quad (5)$$

Let us inspect the three terms above. As there is only one electron per flavor, only inter-flavor terms ($\sigma \neq \sigma'$) survive in

$$J_{ee}(\mathbf{R}_e) = \exp \left[-(1/2) \sum_{\sigma \neq \sigma'} \sum_{i_{e,\sigma}, j_{e,\sigma'}} u_{e,\sigma; e,\sigma'} (|\mathbf{r}_{i_{e,\sigma}} - \mathbf{r}_{j_{e,\sigma'}}|) \right], \quad (6)$$

and in fact the sum over $i_{e,\sigma}$ and $j_{e,\sigma'}$ in the equation above has just one term; so

$$J_{ee}(\mathbf{R}_e) = \exp \left[-(1/2) \sum_{\sigma \neq \sigma'} u_{e,\sigma; e,\sigma'} (|\mathbf{r}_{i_{e,\sigma}} - \mathbf{r}_{j_{e,\sigma'}}|) \right] \equiv \exp \left[\sum_{\sigma < \sigma'} \phi (|\mathbf{r}_{i_{e,\sigma}} - \mathbf{r}_{j_{e,\sigma'}}|) \right], \quad (7)$$

where we have chosen the inter-flavor pseudopotentials all equal, $u_{e,\sigma';e,\sigma'}(r) = \phi(r)$. Since we are considering a paramagnetic, symmetric bilayer it immediately follows that

$$J_{hh}(\mathbf{R}_h) = \exp \left[\sum_{\sigma < \sigma'} \phi(|\mathbf{r}_{i_{h\sigma}} - \mathbf{r}_{j_{h,\sigma'}}|) \right]. \quad (8)$$

We note that with the choices made the product $J_{ee}(\mathbf{R}_e)J_{hh}(\mathbf{R}_h)$ is symmetric under any electron-hole pair exchange as well as under electrons-holes exchange. Let us turn now to $J_{eh}(\mathbf{R}_e, \mathbf{R}_h)$. We have

$$\begin{aligned} J_{eh}(\mathbf{R}_e, \mathbf{R}_h) &= \exp \left[- \sum_{\sigma, \sigma'} \sum_{i_{e,\sigma}, j_{h,\sigma'}} u_{e,\sigma;h,\sigma'}(|\mathbf{r}_{i_{e\sigma}} - \mathbf{r}_{j_{h,\sigma'}}|) \right] \\ &= \exp \left[- \sum_{\sigma} \sum_{i_{e,\sigma}, j_{h,\sigma}} u_{e,\sigma;h,\sigma}(|\mathbf{r}_{i_{e\sigma}} - \mathbf{r}_{j_{h,\sigma}}|) - \sum_{\sigma \neq \sigma'} \sum_{i_{e,\sigma}, j_{h,\sigma'}} u_{e,\sigma;h,\sigma'}(|\mathbf{r}_{i_{e\sigma}} - \mathbf{r}_{j_{h,\sigma'}}|) \right] \\ &\equiv \exp \left[- \sum_{\sigma} \sum_{i_{e,\sigma}, j_{h,\sigma}} \psi(|\mathbf{r}_{i_{e\sigma}} - \mathbf{r}_{j_{h,\sigma}}|) - \sum_{\sigma \neq \sigma'} \sum_{i_{e,\sigma}, j_{h,\sigma'}} \tilde{\psi}(|\mathbf{r}_{i_{e\sigma}} - \mathbf{r}_{j_{h,\sigma'}}|) \right]. \quad (9) \end{aligned}$$

Above we have chosen one pseudo potential for electron-hole pairs with the same flavor, $u_{e,\sigma;h,\sigma}(r) = \psi(r)$, and another for electron-hole pairs with different flavor, $u_{e,\sigma;h,\sigma'}(r) = \tilde{\psi}(r)$. The possibility of $\tilde{\psi}(r)$ being different from $\psi(r)$ should allow the fragmentation of the polyexcitons in smaller components, namely excitons [13,15]. This choice, however, breaks the symmetry under electron-electron pair exchange, as is clear by inspecting eq. (9). Thus we restore the symmetry by taking the symmetrized version of $J_{eh}(\mathbf{R}_e, \mathbf{R}_h)$

$$J_{eh}^S(\mathbf{R}_e, \mathbf{R}_h) = \sum_{\hat{P}_e} \hat{P}_e \exp \left[- \sum_{\sigma} \sum_{i_{e,\sigma}, j_{h,\sigma}} \psi(|\mathbf{r}_{i_{e\sigma}} - \mathbf{r}_{j_{h,\sigma}}|) - \sum_{\sigma \neq \sigma'} \sum_{i_{e,\sigma}, j_{h,\sigma'}} \tilde{\psi}(|\mathbf{r}_{i_{e\sigma}} - \mathbf{r}_{j_{h,\sigma'}}|) \right] \quad (10)$$

where \hat{P}_e permutes the electron coordinates. Finally, the trial wave function

$$\Psi_{NX}^T(\mathbf{R}_e, \mathbf{R}_h) = J_{ee}(\mathbf{R}_e)J_{hh}(\mathbf{R}_h)J_{eh}^S(\mathbf{R}_e, \mathbf{R}_h) \quad (11)$$

is nodeless and satisfies all the required symmetry properties: symmetry under pair exchange of electrons (holes), symmetry under exchange of electrons and holes. We note that in the unsymmetrized electron-hole Jastrow of eq. (9) the pseudopotential $\psi(r)$ describes intra-exciton correlations while $\tilde{\psi}(r)$ describes inter-exciton correlations.

We take the pseudopotentials of the Padé form. For the electron-electron (hole-hole):

$$\phi(r) = \frac{c_1 r}{1 + c_2 r}. \quad (12)$$

For the electron-hole:

$$\psi(r) = \frac{c_3 r + c_4 r^2}{1 + c_5 r}, \quad (13)$$

$$\tilde{\psi}(r) = \frac{c_3 r + c_6 r^2}{1 + c_7 r}. \quad (14)$$

The parameters $c_1 - c_7$ are either fixed by exact conditions or determined through energy minimization as follows. The parameter c_1 is fixed by the electron-electron (hole-hole) Kato cusp conditions [23]. The parameter c_3 is fixed by the electron-hole cusp condition at $d = 0$, while for $d > 0$ there is no electron-hole cusp and so we set $c_3 = 0$ [13]. We require $c_2, c_5, c_7 > 0$ to avoid divergences and $c_4, c_6 < 0$ to describe the wavefunction decay when electron and hole are far apart. The above wave function should describe separated excitons when either c_4 or c_6 goes to zero.

2.2. Exciton wave function

The Schrödinger equation for the ground state of the isolated exciton, in the center-of-mass reference frame, reads

$$\left[-\frac{2}{r} \frac{\partial}{\partial r} \left(r \frac{\partial}{\partial r} \right) + \frac{2}{\sqrt{r^2 + d^2}} \right] \Phi_X^0(r) = E_X^0 \Phi_X^0(r), \quad (15)$$

with $r = |\mathbf{r}_e - \mathbf{r}_h|$ the in-plane distance between electron and hole. At $d = 0$ eq. (15) has the simple hydrogenic normalized solution $\Phi_X^0(r) = \sqrt{2/\pi} \exp[-r]$, with energy $E_X^0(Ry^*) = -2$. However, at $d > 0$ there is no closed form for the solution, which must be computed numerically. To this end we have used the simple and accurate Numerov algorithm [24], which is especially suited for atomic like problems.

3. Results

In Table 1 we report the ground state energy per particle of the exciton, biexciton, and quadriexciton as function of the inter-layer distance d . The energies of the biexciton and quadriexciton were obtained by DMC simulations using as guiding function the optimized trial function of eq. (11). The optimisation with respect to the free parameters was performed by minimising the variational energy using the linear method [25,26] and checking, in selected cases, that the obtained minimum agrees with the one found by the improved stochastic reconfiguration method [27]. DMC simulations are affected by walker population bias (finite number of walkers N_w) and finite timestep bias. However for small systems, such as those studied here, these biases can be easily made negligible. To this end we have used a large number of walkers, $N_w = 1760$, and performed extrapolation to zero timestep. A good optimisation and bias reduction are especially important when estimating pair-correlation functions.

From Table 1 it is evident that for $d = 0$ we have $E_X/2 > E_{2X}/4 > E_{4X}/8$ and that with increasing d the energies of all the three "phases" increase, become closer and could presumably cross or merge. So, studying for instance the stability of the biexciton with respect to the separation into 2 excitons requires extrapolation of the available biexciton energies at larger distances d . In fact a more efficient manner to study the stability of polyexcitons is to define a binding energy with respect to the separation into fragments. The binding energy of a polyexciton is defined as the energy released upon the formation of a bound state with respect to the initially isolated constituents (fragments). Therefore for a biexciton we can define

$$E_B(2X) = 2E_X - E_{2X} \quad (16)$$

and on the same footing the quadriexciton binding energy with respect to two isolated biexcitons is defined as:

$$E_B(4X) = 2E_{2X} - E_{4X}. \quad (17)$$

Table 1. Energy per particle $E_X/2$ (exciton), $E_{2X}/4$ (biexciton), $E_{4X}/8$ (quadriexciton) for various distances d . Excitonic energies are estimated using Numerov algorithm [24]. The energies for the excitonic complexes are obtained from DMC simulations with $N_w = 1760$ walkers and time-step bias removed by extrapolation to zero time-step.

d	$E_X/2$	$E_{2X}/4$	$E_{4X}/8$
0.000	-1.00000000	-1.096435(6)	-1.32793(5)
0.100	-0.76594269	-0.80450(4)	-0.89400(5)
0.200	-0.64517991	-0.66372(1)	-0.70988(3)
0.300	-0.56511027	-0.57420(1)	-0.59997(3)
0.400	-0.50651906	-0.510687(6)	-0.52533(2)
0.500	-0.46112073	-0.46273(1)	-0.47050(1)
0.550	-0.44192983	-0.442815(6)	-0.448179(6)
0.600	-0.42457683	-0.425001(5)	-0.42844(1)
0.650	-0.40878665	-0.408919(7)	-0.410877(6)
0.675	-0.40140710	-0.401466(8)	-0.402841(9)
0.700	-0.39433924	-0.3943676(9)	-0.39498(8)
0.710	-0.39159457	-0.391622(8)	-0.39202(2)
0.720	-0.38889512	-0.3889012(5)	-0.38909(1)
0.740	-0.38362702	-0.3836290(4)	–
0.750	-0.38105610	-0.3810579(5)	–
0.760	-0.37852580	-0.3785260(1)	–
0.780	-0.37358293	-0.37358300(2)	–

3.1. Biexciton binding energy

Meyertholen and Fogler [14] have shown that with increasing the inter-layer distance the binding energy of a biexciton with respect to two excitons vanishes at a finite critical distance d_c and for $d \lesssim d_c$ has the behavior

$$E_B(2X, d) = E_0(d)e^{-D/(d_c-d)}, \quad (18)$$

with

$$E_0(d) = e^{-6\gamma/d^4}, \quad (19)$$

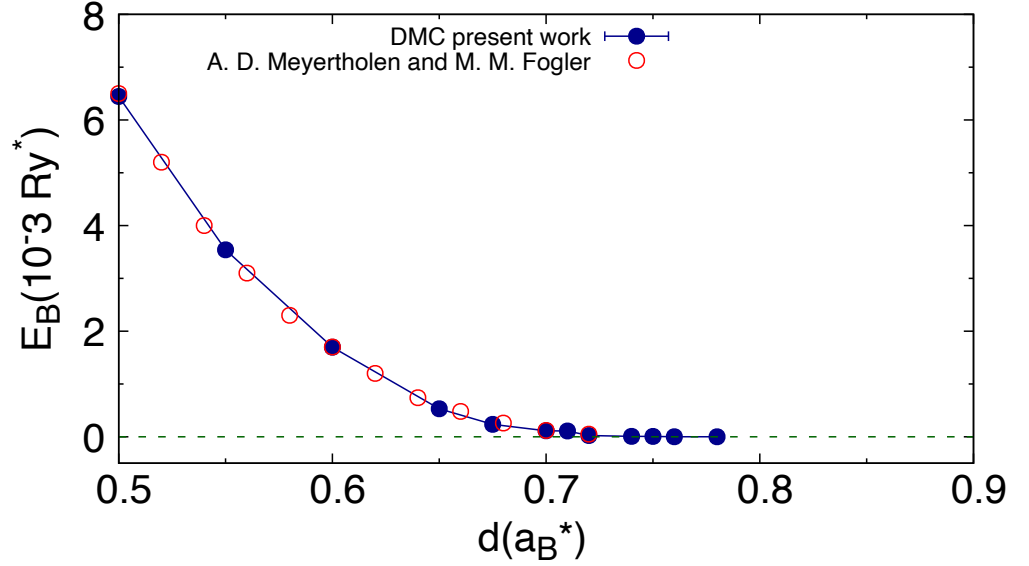


Figure 1. Binding energy $E_B(2X, d)$ of the biexciton as a function of the inter-layer separation d . Together with our results from DMC (solid blue dots), we also report binding energies from Ref. [14] (open red dots). Line joining DMC data are only a guide to the eye.

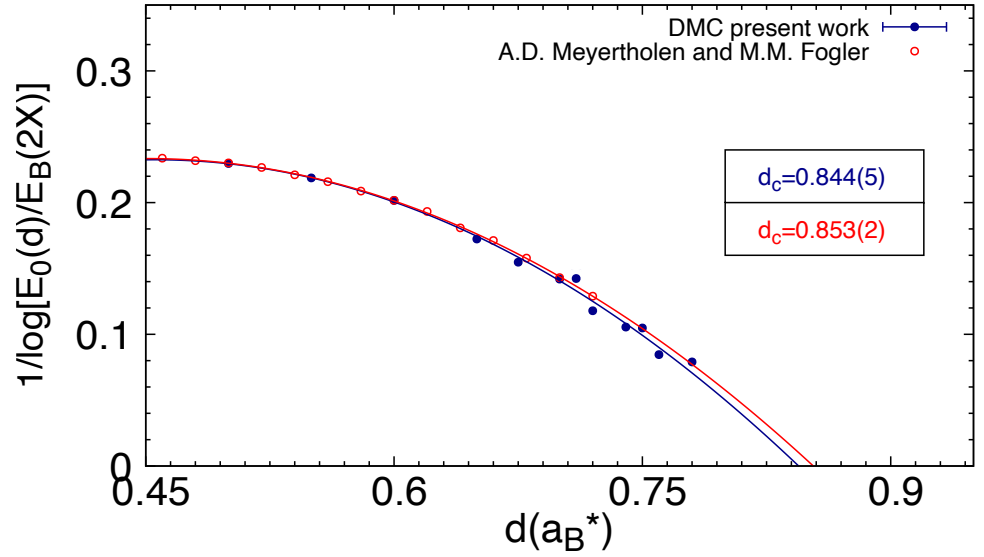


Figure 2. Natural logarithm of binding energy E_B as a function of layer separation d , fitted to the function $1/\log[E_0(d)/E_B(d)] = (d_c - d)/D + (d_c - d)^2/D_1$ as suggested in Ref. [14]. We compare results from our DMC simulation and results from Ref. [14].

D a positive constant of order 1, $\gamma = 0.577\dots$ the Euler-Mascheroni constant and $D/(d_c - d) \gg 1$. Clearly the last condition implies $E_B \ll E_0$. Their derivation is built on the fact that at large d the biexciton is weakly bound and the exciton-exciton interaction brings into play at large inter-exciton distance the dipole-dipole interaction, present for $d > 0$. Clearly the larger is d , the larger is the exciton dipole and the greater is the importance of such interaction.

In brief, they neglect what happens at small inter-excitonic distance and write a Schrödinger equation for two interacting excitons valid at intermediate distance (first region) and at large distance (second region): in the first region the binding energy is neglected with respect to the dipole-dipole interaction and in the second the dipole-dipole interaction is neglected with respect to the binding energy. Imposing the continuity of the logarithmic derivative of the wave function in going from the first to the second region, they obtain an expression involving the binding energy of the biexciton and a characteristic energy of the problem $E_0(d)$. Further manipulations yield finally eq. (18). On the basis of their analysis they propose a fit of the binding energy in the form

$$\frac{1}{\log(E_0(d)/E_B)} = \frac{d_c - d}{D} + \frac{(d_c - d)^2}{D_1}, \quad (20)$$

with d_c, D, D_1 fitting parameters.

In Fig. 1 we report our DMC results for the binding energy $E_B(2X, d)$ of the biexciton, together with the results of the stochastic variational method (SVM) of [14]. In Fig. 2 we report the same data of Fig. 1 in a form suitable for the fit according to eq. (20). One effect of using the "lens" provided by the logarithm is to emphasize the region of distances d near d_c as well as the need of extrapolating to d_c . It is also clear from Fig. 2 that the SVM and DMC results are in good agreement, with the DMC results covering a larger range, which should be important for the fit. Minor differences are found in the values of d_c provided by the fits using the two data sets. We should also stress that in the range of distances covered in Figs. 1 and 2 $E_0(d)$ is at least two orders of magnitude larger than E_B , so that the requirement $E_B \ll E_0$ is fully fulfilled.

3.2. Quadriexciton binding energy

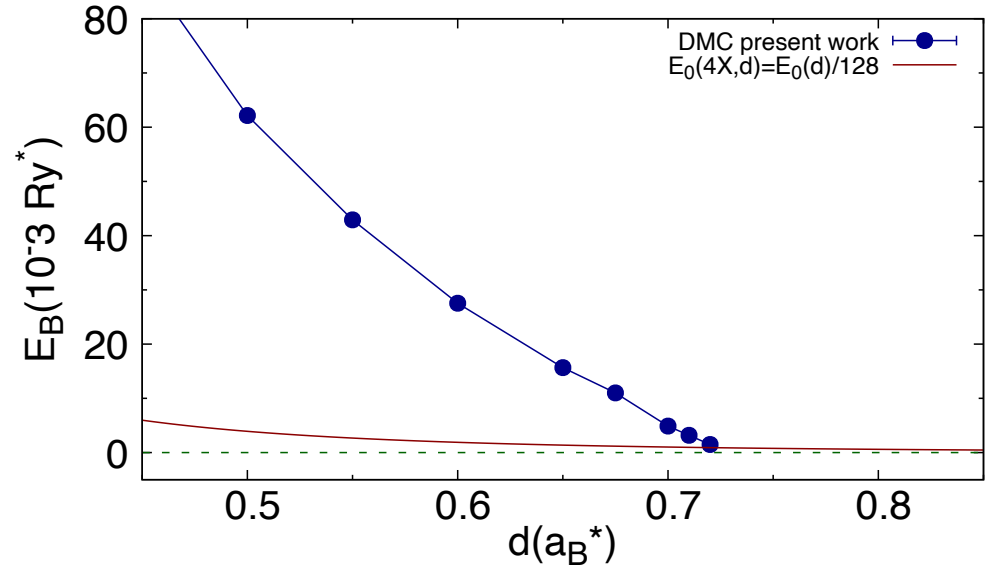


Figure 3. Quadriexciton binding energy E_b as a function of layer separation d . We compare DMC results (solid blue dots) with $E_0(4X, d) = E_0(d)/128$. (solid dark-red line) (19). Line joining DMC data are only guide to the eye.

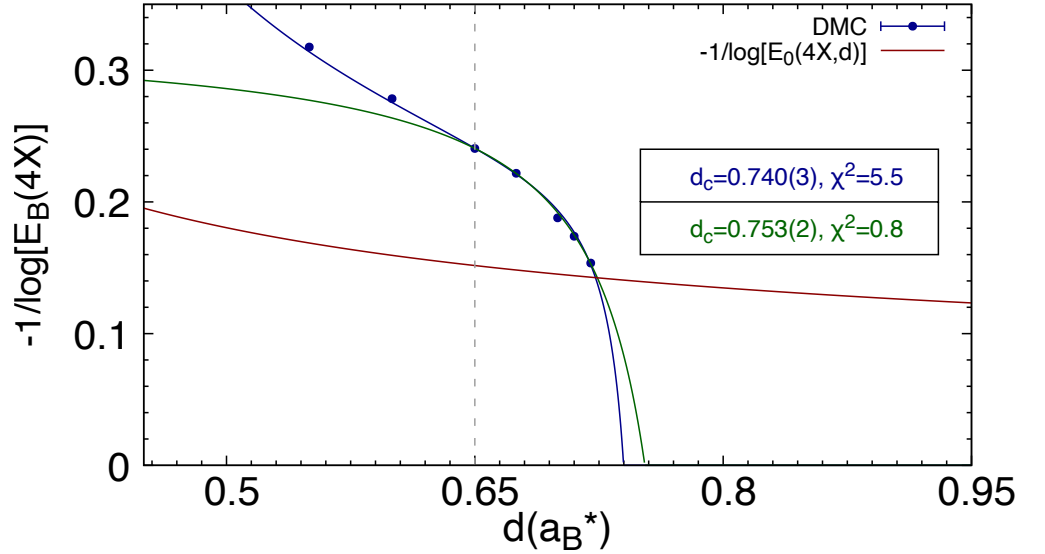


Figure 4. The function $-1/\log(E_B(4X, d))$ (solid blue dots) is compared with $-1/\log[E_0(4X, d)]$ (solid dark-red line). We show fits using the DMC data in the range from $d = 0.65$ to the functions $f(d) = (A/d^4)e^{-D/(d_c-d)}$ (solid blue line) and $q(d) = Ae^{-b/(d_c-d)}$ (solid dark-green line). In the box we report the values of the critical distances according to the two fitting functions, together with the reduced χ^2 .

In principle one may study the quadriexciton stability following the treatment for the biexciton and assuming that also for the quadriexciton the binding energy vanishes at a finite critical distance d_c . So, at distances $d \lesssim d_c$ the quadriexciton is weakly bound and the biexciton-biexciton interaction (dipole-dipole interaction), comes into play. The Schrödinger equation for the relative motion of the two interacting biexcitons is similar to the one for the two interacting excitons, with the following differences. With respect to the exciton-exciton case, the reduced mass is twice larger and the dipole-dipole coupling is 4 times larger. This yields, when imposing the continuity of the logarithmic derivative of the wave function at large distances (see the biexciton case above) an expression involving the ratio of the binding energy of the quadriexciton $E_B(4X, d)$ and a characteristic energy of the problem which turns out to be $E_0(4X, d) = E_0(d)/128$, with $E_0(d)$ given in eq. (19). However the self-consistency of the procedure would require $E_B(4X, d) \ll E_0(4X, d)$, a condition which is not fulfilled in the present case, as is clear from Fig. 3, where our DMC results for $E_B(4X, d)$ are displayed together with $E_0(4X, d)$. We therefore try fit functions different from the one used for the biexciton and given in eq. 20). The first choice is

$$q(d) = Ae^{-D/(d_c-d)}; \quad (21)$$

the second, more flexible, substitutes A with the function A/d^4 ; in both cases A , D and d_c are the fitting parameters.

$$f(d) = (A/d^4)e^{-D/(d_c-d)}; \quad (22)$$

The results of the fits to our DMC energies are displayed in in Fig. ?? in terms of the logarithm of $E_B(4X, d)$, to exploit the "lens" effect. The two different recipes (the second somewhat inspired by the biexciton fit function) give compatible results as far as the d_c value

is concerned. However the second choice reproduces DMC energies in a larger interval of distances, i.e., also energies that were not included in the fitting.

3.3. Quadriexciton pair correlation functions

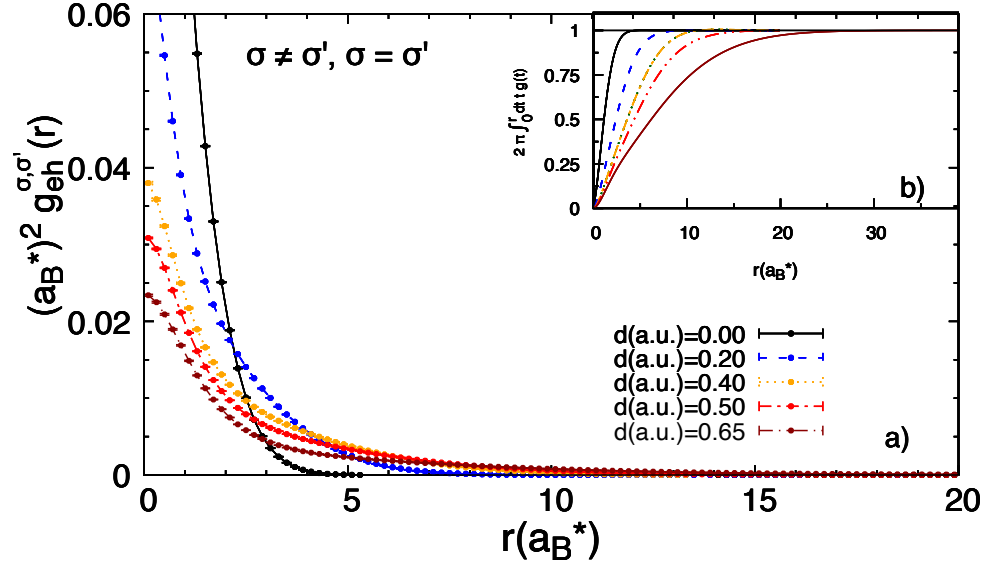


Figure 5. Electron-hole pair-correlation functions for the quadriexciton at several distances d . In panel a) extrapolated DMC $g_{eh}(r)$ are shown for distances $d = 0.0, 0.2, 0.4, 0.5$ and 0.65 (a.u.) with black, blue, orange, red and dark-red solid points, respectively. Lines joining DMC data are only guide to the eye. In panel b) we show the quantity $2\pi \int_0^r dt t g(t)$ that sums up to 1 in all cases for the r -ranges considered here.

In a finite system pair correlation functions can be defined as appropriate "center-of-mass" averages of the two-body density. Lets consider electron-electron correlations. As we have four electrons (one per flavor) we can start from the two-body electron-electron density

$$\rho_{ee}^{\sigma\sigma'}(\mathbf{r}_1, \mathbf{r}_2) = \langle \delta(\mathbf{r}_1 - \mathbf{r}_{e,\sigma}) \delta(\mathbf{r}_2 - \mathbf{r}_{e,\sigma'}) \rangle, \quad (23)$$

where $\langle \dots \rangle$ indicates a ground state average and only the different-flavor case is present. We define new vectors as $\mathbf{R} = (\mathbf{r}_1 + \mathbf{r}_2)/2$ and $\mathbf{r} = \mathbf{r}_1 - \mathbf{r}_2$, so that $\mathbf{r}_1 = \mathbf{R} + \mathbf{r}/2$ and $\mathbf{r}_2 = \mathbf{R} - \mathbf{r}/2$. Substituting in eq. (23) we get

$$\rho_{ee}^{\sigma\sigma'}(\mathbf{R} + \mathbf{r}/2, \mathbf{R} - \mathbf{r}/2) = \langle \delta(\mathbf{R} + \mathbf{r}/2 - \mathbf{r}_{e,\sigma}) \delta(\mathbf{R} - \mathbf{r}/2 - \mathbf{r}_{e,\sigma'}) \rangle, \quad (24)$$

and integrating over the "center-of-mass" vector \mathbf{R} we obtain a pair correlation function

$$g_{ee}^{\sigma\sigma'}(\mathbf{r}) = \langle \delta(\mathbf{r} - \mathbf{r}_{e,\sigma} + \mathbf{r}_{e,\sigma'}) \rangle. \quad (25)$$

Few observations are in order. First $g_{ee}^{\sigma\sigma'}(\mathbf{r})$ is a dimensional quantity; it has the dimensions of a density. However for our finite system there is no sensible density to divide by to get a dimensionless pair correlation function, as in extended systems. The integration of $g_{ee}^{\sigma\sigma'}(\mathbf{r})$ with respect to \mathbf{r} over all space is 1. One usually finds convenient to take the angles average

of $g_{ee}^{\sigma\sigma'}(\mathbf{r})$ to get a $g_{ee}^{\sigma\sigma'}(r)$. In a similar manner one may define electron-hole pair correlation functions as

$$g_{eh}^{\sigma\sigma'}(\mathbf{r}) = \langle \delta(\mathbf{r} - \mathbf{r}_{e,\sigma} + \mathbf{r}_{h,\sigma'}) \rangle, \quad (26)$$

having in this case both same-flavor $\sigma' = \sigma$ and different flavor $\sigma' \neq \sigma$ functions. We should mention that the above definitions for the pair correlation functions coincide with that of the intracule density in chemistry as defined in [28].

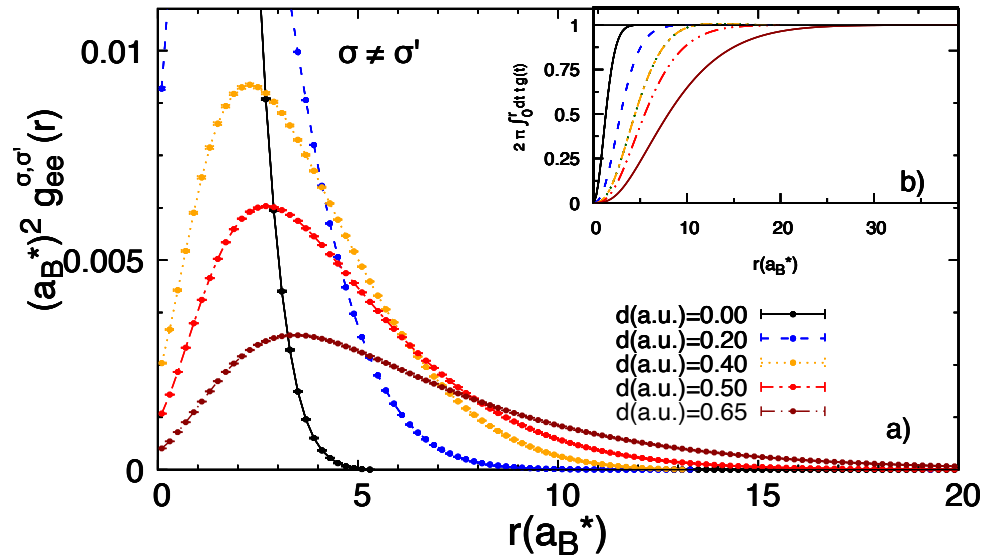


Figure 6. Electron-electron pair-correlation functions for the quadriexciton at several distances d . In panel *a*) extrapolated DMC $g_{ee}(r)$ are shown for distances $d = 0.0, 0.2, 0.4, 0.5$ and 0.65 (*a.u.*) with black, blue, orange red and dark-red solid points, respectively. Lines joining DMC data are only guide to the eye. In panel *b*) we shown the quantity $2\pi \int_0^r dt t g(t)$ that sums up to 1 in all cases for the r -ranges considered here.

In Fig. 5 we show the electron-hole pair correlation functions, at various distances d , averaged on the azimuthal angle. Clearly the contact value $g_{eh}^{\sigma\sigma'}(r=0)$ is a decreasing function of d . At the largest d shown ($d = 0.65$) there is still an appreciable pile up of probability at the origin. In Fig. 6 we show the electron-electron pair correlation functions. A peak, at distances on the scale of a few Bohr radii, is present, due to the quadriexciton binding; similarly to what happens to the contact values of $g_{eh}^{\sigma\sigma'}(r)$, such a peak is a decreasing function of d . Our results are similar to those in [15] for the biexciton. One should keep in mind that different units are used in the two studies, so our pair correlation functions should be multiplied by 4, before comparing with those of the biexciton case in [15]. Finally, as a symmetry check, we have verified that electron-hole pair correlation functions with the same or different flavor coincide; similarly electron-electron pair correlation functions do not depend on the pair of different flavors chosen.

4. Discussion

We have studied a system of 4 electrons and 4 holes (quadriexciton) in a symmetric, paramagnetic bilayer, where indirect excitons are formed, focussing on (i) the unbinding of the quadriexciton into 2 biexcitons and (ii) the pair correlation functions. To this end we have used state-of-the-art QMC simulations in which both quadriexcitons and biexcitons have been

studied. We have already analyzed the various properties of biexcitons and quadriexcitons in the foregoing. Here we shall just discuss what are the implications of our results and analysis in relation to the phase diagram of the symmetric, paramagnetic bilayer at finite density [17,18].

According to our analysis and the one in [14], an isolated biexciton unbinds into 2 excitons at $d_c = 0.84a_B^*$. Evidently one might speculate that such result could be of some relevance to the condensed phase, though only at very small density. The phase diagram in [17] covers the density range $0 \leq r_s \leq 8$ and reveals a biexcitonic phase only for $4 \lesssim r_s \lesssim 8$ and $d \lesssim d_{2X}(r_s) = 0.05a_B^*$. One may therefore conclude that at such densities the electronic screening is very effective in destabilizing the biexcitonic phase and favoring its melting into excitons; to the point that the biexcitonic phase almost disappears. The situation appears qualitatively different in the symmetric, paramagnetic bilayer with valley degeneracy [18]. In this system a robust quadriexcitonic phase is present in the same density range $0 \leq r_s \leq 8$. It first appears around $r_s = 1.5$ at $d = 0$ but with increasing r_s the quadriexciton-exciton boundary increases up to $d \simeq 0.65a_B^*$ at $r_s = 8$. This d value is just 12% smaller than the $d = 0.74a_B^*$ at which the isolated quadriexciton melts into 2 biexcitons. One may then observe, comparing Fig. 1 and 3, that the binding energy of the quadriexciton is about one order of magnitude larger than that of the biexciton for $0.5a_B^* \leq d \leq 0.65a_B^*$. Is that the reason of the much greater stability of quadriexciton in the condensed phase, as compared with the biexciton? We plan to study farther the properties of polyexcitons, in the near future, to answer this and other questions.

Author Contributions: "Conceptualization, G.S. and S.D.P. ; methodology, G. S. and S.D.P. ; investigation, S.D.P. and C. M. " All the authors discussed the details of the work and contributed to the writing of the paper. All authors have read and agreed to the published version of the manuscript.

Funding: "This research received no external funding"

Data Availability Statement: Data are available on request

Acknowledgments:

Conflicts of Interest: The authors declare no conflict of interest.

References

1. Ashcroft, Neil W.; Mermin, D.N. *Solid State Physics*; Holt, Rinehart and Winston: New York, 1976.
2. Here we are interested in Mott-Wannier excitons.
3. Lampert, M.A. Mobile and Immobile Effective-Mass-Particle Complexes in Nonmetallic Solids. *Phys. Rev. Lett.* **1958**, *1*, 450–453. <https://doi.org/10.1103/PhysRevLett.1.450>.
4. Moskalenko, S.A. *Zh. Opt. Spektrosk.* **1958**, *5*, 147.
5. Ihn, T. *Semiconductor Nanostructures*; Oxford University Press: Oxford, 2010.
6. Wang, J.S.Y.; Kittel, C. Excitonic molecules: A possible new form of chemical bonding. *Physics Letters A* **1972**, *42*, 189 – 190. [https://doi.org/https://doi.org/10.1016/0375-9601\(72\)90854-7](https://doi.org/https://doi.org/10.1016/0375-9601(72)90854-7).
7. Perali, A.; Neilson, D.; Hamilton, A.R. High-Temperature Superfluidity in Double-Bilayer Graphene. *Phys. Rev. Lett.* **2013**, *110*, 146803. <https://doi.org/10.1103/PhysRevLett.110.146803>.
8. Li, J.I.A.; Taniguchi, T.; Watanabe, K.; Hone, J.; Levchenko, A.; Dean, C.R. Negative Coulomb Drag in Double Bilayer Graphene. *Phys. Rev. Lett.* **2016**, *117*, 046802. <https://doi.org/10.1103/PhysRevLett.117.046802>.
9. Lee, K.; Xue, J.; Dillen, D.C.; Watanabe, K.; Taniguchi, T.; Tutuc, E. Giant Frictional Drag in Double Bilayer Graphene Heterostructures. *Phys. Rev. Lett.* **2016**, *117*, 046803. <https://doi.org/10.1103/PhysRevLett.117.046803>.
10. Liu, X.; Watanabe, K.; Taniguchi, T.; Halperin, B.I.; Kim, P. Quantum Hall drag of exciton condensate in graphene. *Nat Phys* **2017**, *13*, 746–750.
11. Li, J.I.A.; Taniguchi, T.; Watanabe, K.; Hone, J.; Dean, C.R. Excitonic superfluid phase in double bilayer graphene. *Nat Phys* **2017**, *13*, 751–755.

12. Burg, G.W.; Prasad, N.; Kim, K.; Taniguchi, T.; Watanabe, K.; MacDonald, A.H.; Register, L.F.; Tutuc, E. Strongly Enhanced Tunneling at Total Charge Neutrality in Double-Bilayer Graphene-WSe₂ Heterostructures. *Phys. Rev. Lett.* **2018**, *120*, 177702. <https://doi.org/10.1103/PhysRevLett.120.177702>.
13. Tan, M.Y.J.; Drummond, N.D.; Needs, R.J. Exciton and biexciton energies in bilayer systems. *Phys. Rev. B* **2005**, *71*, 033303. <https://doi.org/10.1103/PhysRevB.71.033303>.
14. Meyertholen, A.D.; Fogler, M.M. Biexcitons in two-dimensional systems with spatially separated electrons and holes. *Phys. Rev. B* **2008**, *78*, 235307. <https://doi.org/10.1103/PhysRevB.78.235307>.
15. Lee, R.M.; Drummond, N.D.; Needs, R.J. Exciton-exciton interaction and biexciton formation in bilayer systems. *Phys. Rev. B* **2009**, *79*, 125308. <https://doi.org/10.1103/PhysRevB.79.125308>.
16. De Palo, S.; Rapisarda, F.; Senatore, G. Excitonic Condensation in a Symmetric Electron-Hole Bilayer. *Phys. Rev. Lett.* **2002**, *88*, 206401. <https://doi.org/10.1103/PhysRevLett.88.206401>.
17. Maezono, R.; López Ríos, P.; Ogawa, T.; Needs, R.J. Excitons and biexcitons in symmetric electron-hole bilayers. *Phys. Rev. Lett.* **2013**, *110*, 216407. <https://doi.org/10.1103/PhysRevLett.110.216407>.
18. De Palo, S.; Tramonto, F.; Moroni, S.; Senatore, G. Quadriexcitons and excitonic condensate in a symmetric electron-hole bilayer with valley degeneracy. *Phys. Rev. B* **2023**, *107*, L041409. <https://doi.org/10.1103/PhysRevB.107.L041409>.
19. Reynolds, P.J.; Ceperley, D.M.; Alder, B.J.; Lester, W.A. Fixed-node quantum Monte Carlo for molecules. *The Journal of Chemical Physics* **1982**, *77*, 5593–5603. <https://doi.org/10.1063/1.443766>.
20. Umrigar, C.J.; Nightingale, M.P.; Runge, K.J. A diffusion Monte Carlo algorithm with very small time-step errors. *J. Chem. Phys.* **1993**, *99*, 2865–2890, [<https://doi.org/10.1063/1.465195>]. <https://doi.org/10.1063/1.465195>.
21. Foulkes, W.M.C.; Mitas, L.; Needs, R.J.; Rajagopal, G. Quantum Monte Carlo simulations of solids. *Rev. Mod. Phys.* **2001**, *73*, 33–83. <https://doi.org/10.1103/RevModPhys.73.33>.
22. We have used the linear method [25,26] and checked, in selected cases, that the obtained minimum agrees with the one found by the improved stochastic reconfiguration method [27].
23. Kato, T. On the eigenfunctions of many-particle systems in quantum mechanics. *Communications on Pure and Applied Mathematics* **1957**, *10*, 151–177. <https://doi.org/10.1002/cpa.3160100201>.
24. See, e.g., [?], sec. 3.3; see also "https://en.wikipedia.org/wiki/Numerov%27s_method".
25. Toulouse, J.; Umrigar, C.J. Optimization of quantum Monte Carlo wave functions by energy minimization. *J. Chem. Phys.* **2007**, *126*, 084102. <https://doi.org/10.1063/1.2437215>.
26. Umrigar, C.J.; Toulouse, J.; Filippi, C.; Sorella, S.; Hennig, R.G. Alleviation of the Fermion-Sign Problem by Optimization of Many-Body Wave Functions. *Phys. Rev. Lett.* **2007**, *98*, 110201. <https://doi.org/10.1103/PhysRevLett.98.110201>.
27. Sorella, S.; Casula, M.; Rocca, D. Weak binding between two aromatic rings: Feeling the van der Waals attraction by quantum Monte Carlo methods. *J. Chem. Phys.* **2007**, *127*, 014105, [<https://doi.org/10.1063/1.2746035>]. <https://doi.org/10.1063/1.2746035>.
28. Toulouse, J.; Assaraf, R.; Umrigar, C.J. Zero-variance zero-bias quantum Monte Carlo estimators of the spherically and system-averaged pair density. *The Journal of Chemical Physics* **2007**, *126*, 244112, [<https://doi.org/10.1063/1.2746029>]. <https://doi.org/10.1063/1.2746029>.